Performance of a fixed-bed biofilm reactor with microbubble aeration in aerobic wastewater treatment

Lei Zhang, Junliang Liu, Chun Liu, Jing Zhang and Jingliang Yang

ABSTRACT

Microbubble aeration is supposed to be highly efficient for oxygen supply in aerobic wastewater treatment. In the present study, the performance of a fixed-bed biofilm reactor microbubble-aerated using a Shirasu porous glass (SPG) membrane system was investigated when treating synthetic municipal wastewater. The biofilm formation on the carriers was enhanced with microbubble aeration due to the strong adhesion of microbubbles to the solid surface. The dissolved oxygen concentration, the removals of chemical oxygen demand (COD) and nitrogen, and the oxygen utilization efficiency were influenced by the organic loading rate at a certain oxygen supply capacity. The relatively optimal organic loading rate was determined as 0.82 kgCOD/(m^3 d) when the oxygen supply capacity was 0.93 kgO_2/(m^3 d), where COD and ammonia removal efficiencies were 91.7% and 53.9%, respectively. The corresponding SPG membrane area-based COD removal capacity was 6.88 kgCOD/(m^2 d). The oxygen utilization efficiency of microbubble aeration was obviously higher compared to conventional bubble aeration. The simultaneous nitrification and denitrification occurred in the biofilm reactor and the total nitrogen removal efficiency of 50.4% was achieved under these conditions. In addition, the increase in air supply capacity of the SPG membrane system was suggested to improve its energy utilization efficiency.

Key words | biofilm, fixed-bed bioreactor, microbubble aeration, operation performance, oxygen utilization, wastewater treatment

Lei Zhang
Junliang Liu
Institute of Urban and Rural Construction,
Agricultural University of Hebei,
Baoding 071001,
China

Lei Zhang
Chun Liu (corresponding author)
Jing Zhang
Jingliang Yang
Pollution Prevention Biotechnology Laboratory of Hebei Province,
School of Environmental Science and Engineering,
Hebei University of Science and Technology,
Yuxiang Road 26#,
Shijiazhuang 050018,
China
E-mail: *liuchun@hebust.edu.cn*

INTRODUCTION

The aerobic bioreactor is the most popular process in wastewater treatment plants, where the aerobic digestion of the contaminants depends on sufficient dissolved oxygen (DO). The high DO concentration could accelerate organic contaminants removal (Liu *et al.* 2008). To promote the aerobic biochemical reaction, the oxygen supply rate has to be fast because of oxygen feed limitation; as a result, a large amount of energy consumption is required for oxygen supply (Fayolle *et al.* 2007). Therefore, the highly efficient oxygen supply methods are expected. Nowadays, microbubble technology has been explored for applications in wastewater treatment (Agarwal *et al.* 2011) which provides a promising solution for efficient oxygen supply in aerobic wastewater treatment. A microbubble is defined as a small bubble with a diameter range of 10–50 μm. Microbubbles have potential advantages for the enhancement of gas-liquid mass transfer, due to their large gas-liquid interfacial area, long residence time in the liquid phase and fast dissolution rate.

The widely used methods of microbubble generation are based on gas-water circulation (Takahashi *et al.* 2003; Takahashi 2005; Chu *et al.* 2008a, 2008b), decompression (Liu *et al.* 2010) and gas-water dispersion process using a certain medium, such as Shirasu porous glass (SPG) membranes (Kukizaki & Goto 2006, 2007; Kukizaki & Baba 2008; Kukizaki & Wada 2008; Kukizaki 2009, 2010). The SPG membrane as a kind of porous glass membrane is prepared based on phase separation of primary Na_2O-CaO-MgO-Al_2O_3-B_2O_3-SiO_2 type glasses and subsequent acid leaching (Kukizaki & Nakashima 2004). SPG membranes find many applications as a dispersion medium in the gas dispersion process for the formation of uniformly sized microbubbles. In the gas-liquid dispersion system, the gas phase is forced through a porous SPG membrane into the continuous liquid phase and uniformly sized microbubbles are formed

doi: 10.2166/wst.2016.187

from the inner surface of the membrane. Three processes are included in this dispersion process for microbubble formation: (1) microbubble formation across the pore; (2) microbubble growth; (3) microbubble detachment. The prominent advantage of this technique is that the resultant bubble size and void fraction are mainly determined by the membrane pore size and membrane area, respectively. This indicates that bubble size and void fraction can be optimized for a large-scale application.

The present applications of microbubble technology for wastewater treatment focus on physical-chemical processes and the enhancement of oxygen or ozone mass transfer has been confirmed (Chu *et al.* 2007, 2008a, 2008b; Kukuzaki *et al.* 2010; Liu *et al.* 2010). However, few applications of microbubble technology have been reported in the aerobic wastewater treatment until now, although some microbubble aerators have been developed (Terasaka *et al.* 2011). Some problems caused by microbubbles and their generation process resulted in the improper operation of the activated sludge-based bioreactor, including sludge breakage and poor sludge settleability. On the other hand, the microbubble aeration seems applicable in a biofilm reactor (Liu *et al.* 2012), because the sludge (microbes) is fixed on the carriers and will not experience the microbubble generation process. Furthermore, another expected advantage of microbubble aeration applied in the biofilm reactor is that microbubble aeration might accelerate the biofilm formation on the carriers, because the microbubbles show the strong adhesion to the solid surface (Yang 2002) and then the attachment of suspended microbes to the surface of the carriers would be enhanced.

The application of microbubble aeration in the biofilm reactor might be a promising solution for the efficient aerobic wastewater treatment but the current research is still inadequate. In the present study, a SPG membrane system was used to generate microbubbles to aerate a fixed-bed biofilm reactor treating synthetic municipal wastewater. The biofilm biomass on the carriers was monitored during the start-up of the bioreactor aerated by microbubbles or coarse bubbles, to illustrate the effect of microbubble aeration on the biofilm formation. Moreover, the performance of the bioreactor with microbubble aeration was investigated in a long-term stable operation at different organic loading rates. The DO concentration, the removals of chemical oxygen demand (COD) and nitrogen, the oxygen utilization efficiency and energy consumption of the experimental system were determined and discussed.

METHODS

SPG membrane system for microbubble aeration

Figure 1 depicts the schematic of the experimental system. A hydrophilic tubular SPG membrane (PJ-500-008N) with the pore size of 0.8 μm was purchased from SPG Technology Co. Ltd (Miyazaki, Japan) to generate air microbubbles. The detailed preparation procedures of the SPG membrane have been described elsewhere (Kukizaki & Nakashima 2004). In this gas-liquid dispersion process for microbubble formation, the compressed air (>0.4 MPa) served as the dispersed gaseous phase and the mixed liquor in the bioreactor served as the continuous liquid phase. The compressed air was introduced on the outside and forced through the membrane pores, while the circulation liquid phase was flowed inside the membrane at a velocity range of 0.73–1.08 m/s, corresponding to a Reynolds number range of 1.01×10^4–1.49×10^4. The air flux was controlled as about 1.29 $m^3/(m^2\ h)$ and the corresponding oxygen supply capacity was 0.93 $kgO_2/(m^3\ d)$. The diameter range of most generated microbubbles in clean water was measured roughly as 20–50 μm under these conditions, and then the average microbubble diameter was determined statistically as 33.8 μm, based on microscope observation and measurement (Chu *et al.* 2007), as shown in Figure 2.

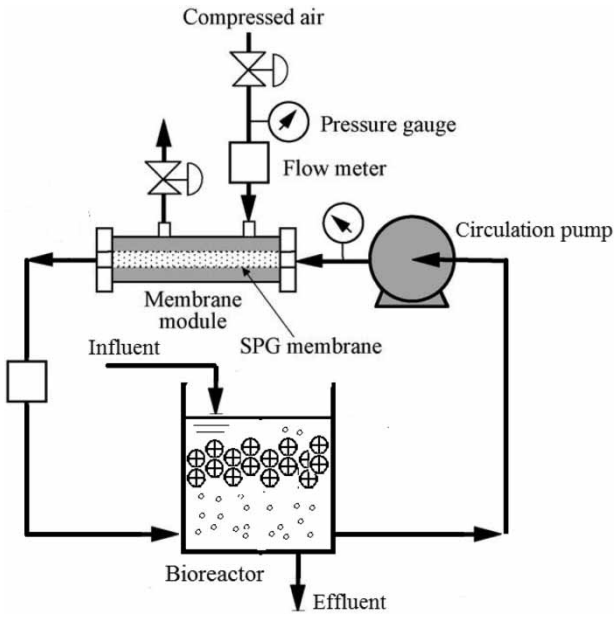

Figure 1 | Schematic diagram of the experimental apparatus.

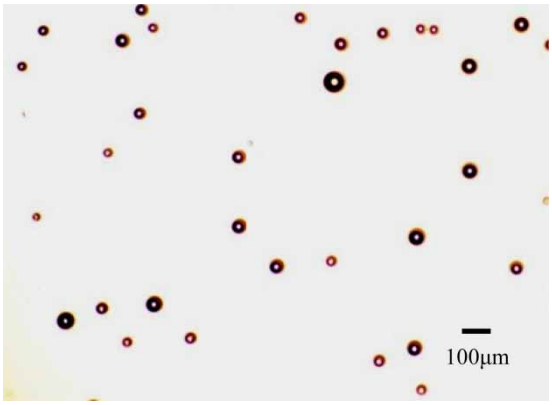

Figure 2 | Observation of microbubbles generated by SPG membrane system in clean water.

Reactor and carriers

The laboratory scale reactor was a transparent plexiglass tank with a diameter of 250 mm and a depth of 600 mm. The work volume of the reactor was 15 L. Three types of the commercial carriers (Shengxing, China) were used in this bioreactor, including porous carrier, ribbon carrier and ring carrier. The porous carrier consisted of about 3.2-cm^3 pieces of a polyurethane cube with pore size of about 1.5 mm. The ribbon carrier consisted of 15-cm-long pieces of a polyethylene ribbon (width 1.0 cm). The ring carrier consisted of 1.5-cm-long pieces of a polypropylene tube (diameter 1.0 cm) with internal longitudinal walls forming a cross inside the carrier. The carriers were filled in polypropylene balls with diameter of 8.0 cm (Figure 3) to construct the fixed bed in the bioreactor, at the carrier filling of about 27%.

Experimental procedure

The SPG membrane system or the usual air distributor was applied in the bioreactor containing three types of the carriers during the start-up period, to provide microbubble aeration or coarse bubble aeration. The activated sludge from a municipal wastewater treatment plant was inoculated into the bioreactor at the mixed liquor suspended solids of 0.8 g/L. A synthetic municipal wastewater was fed into the bioreactor at an organic loading rate of 0.35 kgCOD/(m^3 d). Glucose, starch, peptone, NH_4Cl and KH_2PO_4 were the main constituents in the synthetic wastewater to provide carbon, nitrogen and phosphorus sources (Huang *et al.* 2000). The biomass on the carriers was monitored to compare the biofilm formation, which was measured as biofilm solids (Falås *et al.* 2012). Biofilm solids were determined by the difference in weight of dried carriers (105 °C for >1 h) before and after removal of biofilm. Removal of biofilm solids were made in H_2SO_4 (4 M) through mechanical shaking and ultrasonication, followed by thorough brushing.

After the start-up period, the porous carriers were used in the fixed-bed bioreactor during the long-term stable operation when the dried biofilm solids on the carriers reached to about 1.0 g/L. The SPG membrane system was used for microbubble aeration. The synthetic wastewater mentioned above was treated in the bioreactor. The COD, ammonia and total nitrogen (TN) concentrations of the synthetic wastewater were 377.9 ± 93.7 mg/L, 57.5 ± 15.2 mg/L and 70.2 ± 12.6 mg/L, respectively. Feed wastewater was pumped to the bioreactor continuously and the effluent from the bottom of the reactor was controlled by a valve. The bioreactor was operated at room temperature.

The long-term stable operation of the bioreactor included five phases and the corresponding operating conditions are shown in Table 1. In order to control SPG membrane fouling, the online chemical cleaning was conducted every 2 days, with the procedure of 30 min for the sodium hypochlorite solution (1.3 mol/L), 30 min for the hydrochloric acid solution (0.5 mol/L) and 15 min for water, respectively.

Analytical methods

The DO concentration was determined with an electrochemical membrane electrode (WTW cellOx 325,

Figure 3 | Three types of carriers: (a) porous carrier; (b) ribbon carrier; (c) ring carrier.

Table 1 | Operating conditions

Item	Phase 1	Phase 2	Phase 3	Phase 4	Phase 5
Operation days (d)	1–12	13–32	33–56	57–79	80–94
Air flux ($m^3/(m^2\ h)$)	1.29				
SPG membrane surface area (m^2)	1.57×10^{-3}				3.14×10^{-3}
Oxygen supply capacity ($kgO_2/(m^3\ d)$)	0.93				1.86
Hydraulic retention time (HRT) (h)	24	16	12	8	8
Influent organic loading rate ($kgCOD/(m^3\ d)$)	0.34	0.63	0.82	1.16	1.16

Germany) and a digital DO meter. The air flow rate was determined by a gas flowmeter to calculate air flux. The influent and effluent water testing was conducted on a daily basis for the duration of the experiment. Total COD, ammonia, nitrate and TN were measured in accordance with the standard method. The turbidity was determined using a digital turbidity meter (WGZ-1, Xinrui, China). A single-phase kilowatt hour meter was fitted to the electricity supply to measure the power consumption.

The organic loading rates removed was the COD removal loading rates; it was calculated according to Equation (1).

$$N = \frac{(C_i - C_e)\times 24}{1000T} \tag{1}$$

In Equation (1), N was the organic loading rates removed, $kg/(m^3 d)$; C_i was the COD values of the influent, mg/L; C_e was the COD values of the effluent, mg/L; T was the hydraulic retention time (HRT), h.

The SPG membrane area-based COD removal capacity was calculated according to Equation (2).

$$P = \frac{V(C_i - C_e)\times 24\times 10^{-6}}{AT} \tag{2}$$

In Equation (2), P was the SPG membrane area-based COD removal capacity, $kgCOD/(m^2 d)$; V was the work volume of the reactor, L; C_i was the COD values of the influent, mg/L; C_e was the COD values of the effluent, mg/L; A was the SPG membrane surface area, m^2; T was the hydraulic retention time (HRT), h.

Statistical analyses

Statistical analyses (Pearson correlations) were performed to identify the relationship between different parameters. Pearson correlations indicate the apparent correlations between two variables. Correlation coefficient (R) is indicators of linear estimation which is always between -1 and $+1$. Correlations were considered statistically significant at a 95% confidence interval ($p < 0.05$). All statistical analyses were carried out using SPSS 19.0 software.

RESULTS AND DISCUSSION

Effect of microbubble aeration on biofilm formation

The development of the biofilm biomass on the carriers with the microbubble aeration or the coarse bubble aeration is shown in Figure 4. The fastest biofilm formation was observed on the porous carrier, which seemed independent on the aeration type. The efficient capture of sludge flocs by the porous carrier is considered to be the possible reason for this result due to its dimensional mesh structure.

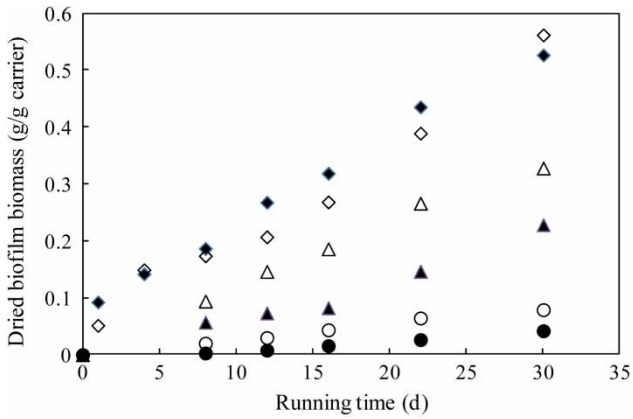

Figure 4 | Comparisons of biofilm formation on the three types of the carriers in both microbubble aeration and coarse bubble aeration: (◇), porous carrier in microbubble aeration; (△), ribbon carrier in microbubble aeration; (○), ring carrier in microbubble aeration; (◆), porous carrier in coarse bubble aeration; (▲), ribbon carrier in coarse bubble aeration; (●), ring carrier in coarse bubble aeration.

On the other hand, the increasing rates of the biofilm biomass on the ribbon carrier and the ring carrier with microbubble aeration were about 50% and 80% faster than those with coarse bubble aeration, respectively. Biofilm formation includes the attachment and growth processes of microbes and it is convinced that the attachment of suspended microbes to the carrier surface is important for the biofilm formation. Therefore, the enhanced attachment of suspended microbes to the carrier surface by microbubbles should be responsible for the faster biofilm formation on the carrier surface in microbubble aeration. The difference in biofilm formation between the ribbon carrier and the ring carrier is probably due to their different shape and surface properties (Hadjiev *et al.* 2007).

DO concentration

The DO concentration in the bioreactor depends on both oxygen transfer and DO utilization by the aerobic digestion. Figure 5 shows the variation of DO concentration in the bioreactor during the long-term stable operation. The declining trend of DO concentration was observed from Phase 1 to Phase 4 due to the increase in organic loading rate at a certain oxygen supply capacity. The average DO concentration decreased from above 5.0 mg/L in Phase 1 to 1.66 mg/L in Phase 4. In addition, the DO concentration showed a significant negative correlation with organic loading rate removed ($R = -0.529$, $p < 0.01$) from Phase 1 to Phase 4, also suggesting the dependence of the DO concentration on the DO utilization by aerobic digestion. Furthermore, the average DO concentration recovered to 2.74 mg/L in Phase 5 at the same organic loading rate with Phase 4, when the air supply capacity was increased by doubling the SPG membrane surface area. This suggests that the membrane area could be optimized for a large-scale application to provide adequate air supply capacity according to the organic loading rate.

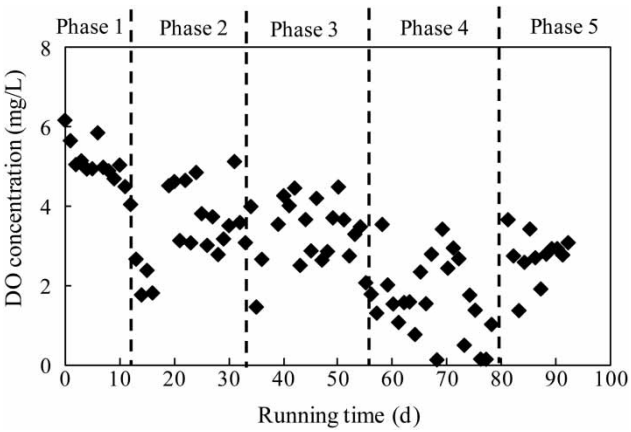

Figure 5 | Dissolved oxygen (DO) concentration with time in the bioreactor.

COD removal

Figure 6(a) shows the COD values of the influent and the effluent of the bioreactor during the long-term stable operation. The average COD values of the effluent in Phases 1, 2, 3, 4 and 5 were 45.1 ± 26.7, 48.6 ± 24.5, 31.0 ± 13.2, 82.5 ± 54.6 and 53.4 ± 21.4 mg/L, respectively. The corresponding COD removal efficiencies were $86.8 \pm 7.5\%$, $87.1 \pm 9.4\%$, $91.7 \pm 3.5\%$, $76.5 \pm 15.0\%$ and $86.2 \pm 5.9\%$, respectively, as shown in Figure 6(b). The organic loading rates removed were 0.29 ± 0.07, 0.54 ± 0.15, 0.72 ± 0.19, 0.84 ± 0.31 and 0.99 ± 0.23 kgCOD/(m^3 d) in Phases 1, 2, 3, 4 and 5, respectively. Then the SPG membrane area-based COD removal capacities were calculated as 2.77, 5.16, 6.88, 8.03 and 4.73 kgCOD/(m^2 d), respectively. These results indicate the proper performance of the prolonged bioreactor with microbubble aeration using the SPG membrane system.

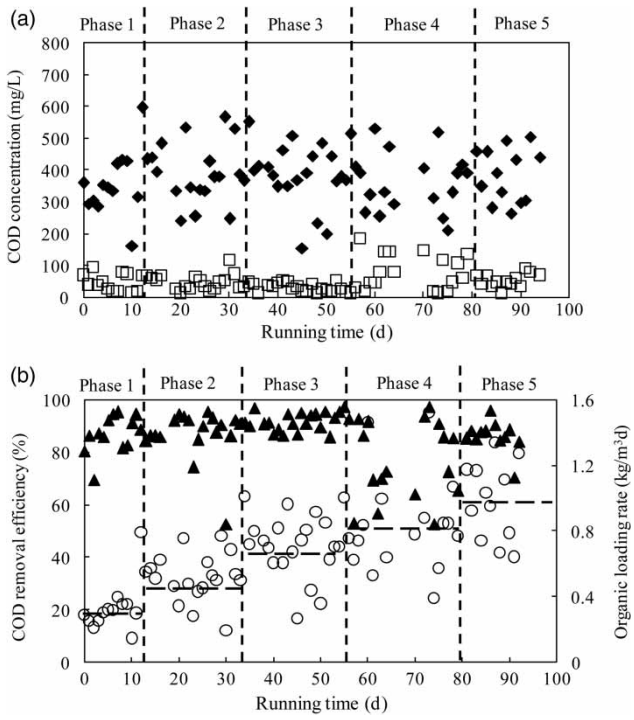

Figure 6 | (a) Time course of COD concentration in the influent and the effluent and (b) time course of COD removal efficiency and organic loading rate removed: (◆) influent; (□) effluent; (▲) COD removal efficiency; (○) organic loading rate removed.

It should be pointed out that the COD removal became inefficient at high organic loading rate in Phase 4 due to inadequate DO for aerobic digestion. Then the maximum and the optimal SPG membrane area-based COD removal capacities under the experimental conditions could be considered as 8.03 kgCOD/(m^2 d) and 6.88 kgCOD/(m^2 d) obtained in Phase 4 and Phase 3, respectively, considering DO concentration and COD removal efficiency. The COD removal capacity depends on the biofilm biomass and the air supply capacity of SPG membrane. When air supply capacity was doubled by increasing SPG membrane area in Phase 5, the DO concentration increased and the COD removal capacity which depends on available DO was also improved to a certain extent. On the other hand, the SPG membrane area-based COD removal capacity decreased in this operation phase, suggesting the biofilm biomass instead of air supply capacity might be the limiting factor of COD removal in this case. Therefore, the air supply capacity should be optimized according to the biofilm capacity and the organic loading rate to improve COD removal capacity and energy efficiency.

Nitrogen removal

Figure 7(a) shows the ammonia values of the effluent and ammonia removal efficiencies in the bioreactor. The relatively efficient ammonia removal was achieved from Phase 1 to Phase 3, and the average ammonia values of the effluent were 8.34 ± 5.0, 14.7 ± 13.5 and 23.5 ± 7.6 mg/L, respectively. The corresponding average ammonia removal efficiencies were $84.1 \pm 6.9\%$, $72.9 \pm 23.9\%$ and $53.9 \pm 14.3\%$, respectively. In addition, the ammonia removal efficiency showed a significant positive correlation with the DO concentration ($R = 0.571$, $p < 0.01$) from Phase 1 to Phase 3, suggesting that the nitrification process was responsible for the ammonia removal mainly, which was strongly DO concentration dependent.

The ammonia removal deteriorated significantly after Phase 3 and the average ammonia removal efficiencies decreased to $21.0 \pm 11.1\%$ and $26.9 \pm 7.6\%$ in Phase 4 and Phase 5, respectively. A reasonable explanation was that the organic loading rate increased and more DO was required for the organic decomposition and, as a result, the available DO for the nitrification became inadequate. In addition, the increased organic loading rate could enhance biofilm growth and increase the thickness of the biofilm. Therefore, the biofilm mass transfer resistance increased which resulted in DO diffusion limitation inside the biofilm. This should be the reason for the inefficient ammonia removal in Phase 5, although the DO concentrations recovered to above 2.0 mg/L (Raunkjær *et al.* 1997).

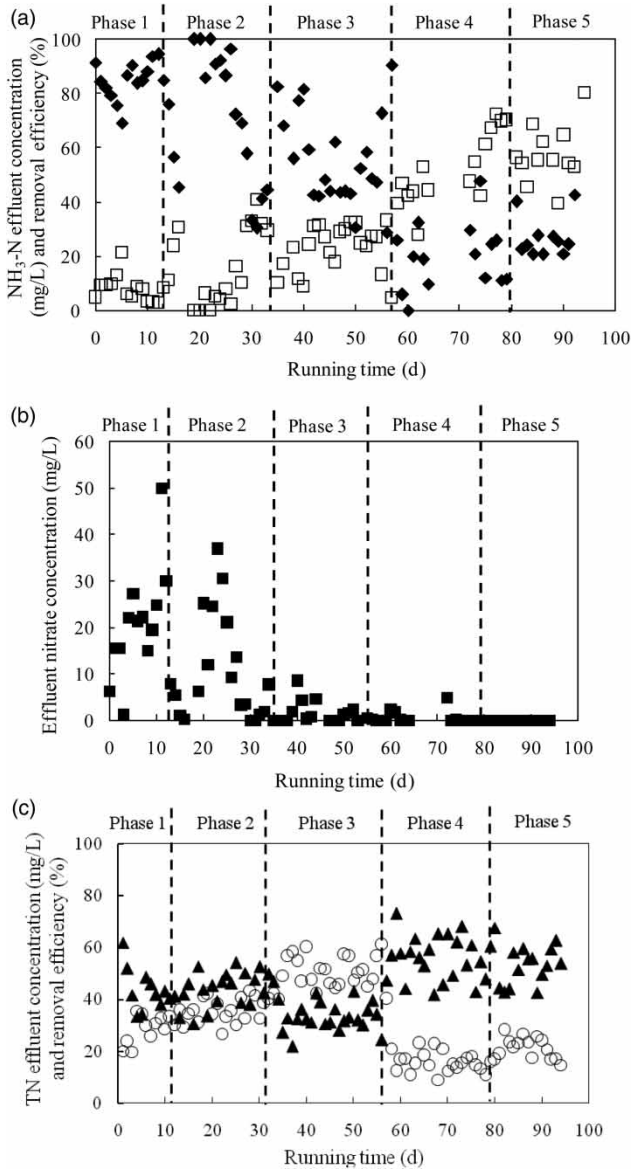

Figure 7 | (a) Time course of ammonia concentration in the effluent and ammonia removal efficiency, (b) time course of nitrate concentration in the effluent and (c) time course of TN concentration in the effluent and TN removal efficiency: (□) effluent ammonia; (◆) ammonia removal efficiency; (■) effluent nitrate; (▲) effluent TN; (○) TN removal efficiency.

The effluent nitrate values of the bioreactor were also monitored to present nitrification and denitrification processes for nitrogen removal, as shown in Figure 7(b). In Phase 1 and Phase 2, the obvious nitrate accumulation was observed and the effluent nitrate values showed a significant positive correlation with the ammonia removal efficiency ($R = 0.473$, $p < 0.05$), indicating that the conversion of ammonia to nitrate due to the nitrification process

was dominant under these conditions. After Phase 2, the effluent nitrate values reduced to almost zero and the ammonia was removed simultaneously, suggesting the simultaneous nitrification and denitrification occurred in the bioreactor. The denitrification occurrence in this aerobic bioreactor was due to the DO diffusion limitation in the biofilm and the consequent anoxic environment inside the biofilm under these conditions.

The TN values of the effluent and TN removal efficiencies in the bioreactor were shown in Figure 7(c). The average TN values of the effluent were 43.4 ± 7.9, 44.1 ± 6.8; 33.8 ± 5.9, 55.9 ± 8.5 and 53.3 ± 7.6 mg/L in Phases 1, 2, 3, 4 and 5, respectively. The denitrification of the nitrate was not obvious in the aerobic environment in Phase 1 and Phase 2, with relatively low TN removal efficiencies of 28.7 ± 5.3% and 35.9 ± 6.8%, respectively. The more efficient TN removal was achieved in Phase 3, with an efficiency of 50.4 ± 16.1%, since the efficient simultaneous nitrification and denitrification occurred in this case, which facilitated the TN removal. However, the TN removal efficiencies in Phase 4 and Phase 5 decreased to 16.5 ± 9.3% and 21.2 ± 8.7%, respectively, because the nitrification process was inhibited, which probably became the rate-limiting step for TN removal.

Turbidity removal

Figure 8 presents the turbidities of the influent and the effluent of the bioreactor during the long-term stable operation. From Phase 1 to Phase 3, the average turbidities of the influent were 14.1 ± 10.7, 17.2 ± 14.0 and 21.4 ± 10.5 NTU, and the corresponding turbidities of the effluent were 6.4 ± 3.5, 6.1 ± 4.8 and 6.4 ± 3.4 NTU, respectively, indicating the relatively efficient turbidity removal in the bioreactor. In Phase 4 and Phase 5, the average turbidity of the effluent increased to 38.2 ± 25.5 and 26.3 ± 15.9 NTU, which was close to or even higher than the influent turbidity of 27.4 ± 16.7 and 31.9 ± 26.3 NTU. The increased turbidity of the effluent in Phase 4 and Phase 5 was due to the enhanced biofilm detachment when the biofilm growth on the carriers was accelerated at the high organic loading rate.

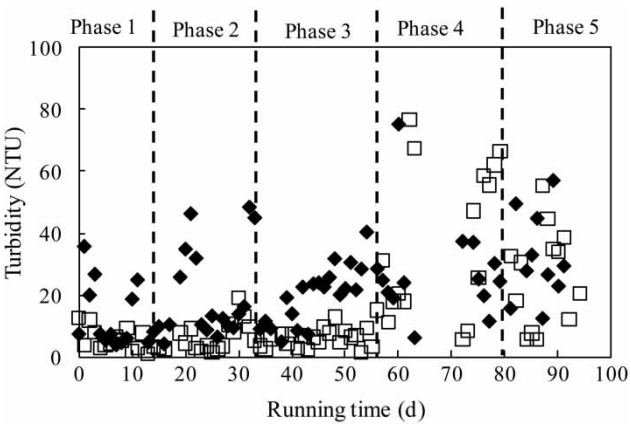

Figure 8 | Time course of turbidity in the influent (◆) and the effluent (□).

Oxygen utilization efficiency

The total volumetric oxygen transfer coefficient, K_La, was determined as about 4.36 h^{-1} when the SPG membrane was used for microbubble aeration in clean water under the same conditions with the bioreactor. The corresponding oxygen transfer efficiency was about 72%, much higher than 15–40% of conventional bubble aeration systems, indicating more efficient oxygen transfer in microbubble aeration.

If only the organic decomposition and the ammonia nitrification were considered for DO utilization in the bioreactor for simplification, the oxygen utilization efficiencies were estimated roughly as 50.8%, 83.8%, 111.9%, 104.3% and 75.7% from Phase 1 to Phase 5, respectively, based on organic and ammonia loading rates removed and the oxygen supply capacity of 0.93 $kgO_2/(m^3$ d). The oxygen utilization efficiency was obviously overestimated. The possible reason was that part of COD and ammonia was not removed by aerobic digestion but by other processes, for example, assimilation of heterotrophic microbes and swallowing of protozoa. Anyway, the microbubble aeration could provide more efficient oxygen utilization in aerobic wastewater treatment, compared to the conventional bubble aeration.

The organic loading rate seems to be an important parameter for the performance of the experimental system. In comparison, the organic loading rate of 0.82 $kgCOD/(m^3$ d) in Phase 3 was relatively optimal under the experimental conditions, where the stable DO concentration, the efficient contaminant removal, the high oxygen utilization efficiency and the suitable biofilm growth could be achieved. Especially, the simultaneous nitrification and denitrification could be realized at this organic loading rate and the efficient TN removal was obtained.

Energy consumption

Almost all microbubble generators require some kinds of mechanical moving parts for microbubble generation, such as pumps, and then the energy consumption of the microbubble generators is convinced to be greater than that of

the usual gas distributors (Terasaka *et al.* 2011). For the SPG membrane system, both a circulation pump and an air compressor are needed for microbubble generation. The power requirement of the SPG membrane microbubble aeration system measured in this case was almost four-fold higher than a conventional bubble aerator, and more than 65% energy consumption was required for the circulation pump. However, the power requirement per unit air supply decreased by more than 40% in Phase 5 when the air supply capacity increased, which suggests that the energy consumption per unit contaminant removal could also decrease significantly. Therefore, to increase the air supply capacity by increasing the area or the air flux of the SPG membrane served by one circulation pump is a possible solution for energy-saving. So for the future application of the SPG membrane microbubble aeration system, it is possible to decrease energy consumption if the system and its operating parameters are optimized.

Although microbubble aeration required a higher energy cost than conventional bubble aeration, oxygen transfer efficiency of microbubble and oxygen utilization efficiency of microbubble aeration was obvious higher. Namely, microbubble aeration can allow downsizing of the aeration tank and shorten the residence time of the wastewater so that a reduction in the overall cost is expected (Terasaka *et al.* 2011).

CONCLUSIONS

The SPG membrane system was applied for microbubble aeration in a fixed-bed biofilm reactor treating synthetic municipal wastewater and its performance was investigated. The strong adhesion of microbubbles to the solid surface facilitated the attachment of suspended microbe to the carrier surface and as a result, the biofilm formation on the carrier was enhanced in microbubble aeration. The DO concentration, the removals of the contaminants and the oxygen utilization efficiency depended on the organic loading rate at a certain oxygen supply capacity. The relatively optimal organic loading rate was determined as 0.82 kgCOD/(m^3 d) when the oxygen supply capacity was 0.93 kgO_2/(m^3 d), and the corresponding SPG membrane area-based COD removal capacity was about 6.88 kgCOD/(m^2 d) with a COD removal efficiency of 91.7%, an ammonia removal efficiency of 53.9% and a roughly estimated oxygen utilization efficiency of almost close to 100%. The simultaneous nitrification and denitrification also occurred at this time and the average TN removal efficiency of 50.4% was achieved. The performance of the bioreactor became inefficient at high organic loading rate due to available DO limitation. On the other hand, the power requirement of the SPG membrane microbubble aeration system was almost four-fold higher than a conventional bubble aerator. The increase in air supply capacity of SPG membrane served by identical circulation pump was suggested to improve energy efficiency.

ACKNOWLEDGEMENT

The authors acknowledge the financial support from Hebei Province Natural Science Foundation of China (E2015208140).

REFERENCES

Agarwal, A., Ng, W. J. & Liu, Y. 2011 Principle and applications of microbubble and nanobubble technology for water treatment. *Chemosphere* **84** (9), 1175–1180.

Chu, L. B., Xing, X. H., Yu, A. F., Zhou, Y. N., Sun, X. L. & Jurcik, B. 2007 Enhanced ozonation of simulated dyestuff wastewater by microbubbles. *Chemosphere* **68** (10), 1854–1860.

Chu, L. B., Yan, S. T., Xing, X. H., Yu, A. F., Sun, X. L. & Jurcik, B. 2008a Enhanced sludge solubilization by microbubble ozonation. *Chemosphere* **72** (2), 205–212.

Chu, L. B., Xing, X. H., Yu, A. F., Sun, X. L. & Jurcik, B. 2008b Enhanced treatment of practical textile wastewater by microbubble ozonation. *Proc. Safety Environ. Protection* **86** (5), 389–393.

Falås, P., Baillon-Dhumez, A., Andersen, H. R., Ledin, A. & la Cour Jansen, J. 2012 Suspended biofilm carrier and activated sludge removal of acidic pharmaceuticals. *Water Res.* **46** (4), 1167–1175.

Fayolle, Y., Cockx, A., Gillot, S., Roustan, M. & Héduit, A. 2007 Oxygen transfer prediction in aeration tanks using CFD. *Chem. Eng. Sci.* **62** (24), 7163–7171.

Hadjiev, D., Dimitrov, D., Martinov, M. & Sire, O. 2007 Enhancement of the biofilm formation on polymeric supports by surface conditioning. *Enzyme Microb. Technol.* **40** (4), 840–848.

Huang, X., Liu, R. & Qian, Y. 2000 Behavior of soluble microbial products in a membrane bioreactor. *Process Biochem.* **36** (5), 401–406.

Kukizaki, M. 2009 Microbubble formation using asymmetric Shirasu porous glass (SPG) membranes and porous ceramic membranes-A comparative study. *Colloids Surf. A: Physicochem. Eng. Asp.* **340** (1–3), 20–32.

Kukizaki, M. 2010 Large-scale production of alkali-resistant Shirasu porous glass (SPG) membranes: Influence of ZrO2 addition on crystallization and phase separation in Na_2O–CaO–Al_2O_3–B_2O_3–SiO_2 glasses; and alkali durability and pore morphology of the membranes. *J. Memb. Sci.* **360** (1–2), 426–435.

Kukizaki, M. & Baba, Y. 2008 Effect of surfactant type on microbubble formation behavior using Shirasu porous glass (SPG) membranes. *Colloids Surf. A: Physicochem. Eng. Asp.* **326** (3), 129–137.

Kukizaki, M. & Goto, M. 2006 Size control of nanobubbles generated from Shirasu-porous-glass (SPG) membranes. *J. Memb. Sci.* **281** (1–2), 386–396.

Kukizaki, M. & Goto, M. 2007 Spontaneous formation behavior of uniform-sized microbubbles from Shirasu porous glass (SPG) membranes in the absence of water-phase flow. *Colloids Surf. A: Physicochem. Eng. Asp.* **296** (1–3), 174–181.

Kukizaki, M. & Nakashima, T. 2004 Acid leaching process in the preparation of porous glass membranes from phase-separated glass in the Na_2O–CaO–MgO–Al_2O_3–B_2O_3–SiO_2 system. *Membrane* **29** (5), 301–308.

Kukizaki, M. & Wada, T. 2008 Effect of the membrane wettability on the size and size distribution of microbubbles formed from Shirasu-porous-glass (SPG) membranes. *Colloids Surf. A: Physicochem. Eng. Asp.* **317** (1–3), 146–154.

Kukuzaki, M., Fujimoto, K., Kai, S., Ohe, K., Oshima, T. & Baba, Y. 2010 Ozone mass transfer in an ozone-water contacting process with Shirasu porous glass (SPG) membranes-A comparative study of hydrophilic and hydrophobic membranes. *Sep Purif. Technol.* **72** (3), 347–356.

Liu, C., Tanaka, H., Zhang, L., Zhang, J., Huang, X., Ma, J. & Matsuzawa, Y. 2012 Fouling and structural changes of Shirasu porous glass (SPG) membrane used in aerobic wastewater treatment process for microbubble aeration. *J. Memb. Sci.* **421–422**, 225–231.

Liu, F., Zhao, C. C., Zhao, D. F. & Liu, G. H. 2008 Tertiary treatment of textile wastewater with combined media biological aerated filter (CMBAF) at different hydraulic loadings and dissolved oxygen concentration. *J. Hazard. Mater.* **160** (1), 161–167.

Liu, S., Wang, Q. H., Ma, H. Z., Huang, P. K., Li, J. & Kikuchi, T. 2010 Effect of micro-bubbles on coagulation flotation process of dyeing wastewater. *Sep. Purif. Technol.* **71** (3), 337–346.

Raunkjær, K., Nielsen, P. H. & Hvitved-Jacobsen, T. 1997 Acetate removal in sewer biofilms under aerobic conditions. *Water Res.* **31** (11), 2727–2736.

Takahashi, M. 2005 Potential of microbubbles in aqueous solutions: electrical properties of the gas-water interface. *J. Phys. Chem. B* **109** (46), 21858–21864.

Takahashi, M., Kawamura, T., Yamamoto, Y., Ohnari, H., Himuro, S. & Shakutsui, H. 2003 Effect of shrinking microbubble on gas hydrate formation. *J. Phys. Chem. B* **107** (10), 2171–2173.

Terasaka, K., Hirabayashi, A., Nishino, T., Fujioka, S. & Kobayashi, D. 2011 Development of microbubble aerator for waste water treatment using aerobic activated sludge. *Chem. Eng. Sci.* **66** (14), 3172–3179.

Yang, C. 2002 Observation of microbubble attachment onto a hydrophilic glass surface. *Chem. Eng. Sci.* **57** (8), 1485–1488.

First received 13 January 2016; accepted in revised form 1 April 2016. Available online 19 April 2016